Published in final edited form as:
*Atherosclerosis*. 2013 December ; 231(2): . doi:10.1016/j.atherosclerosis.2013.09.026.

# Nitric Oxide Improves Molecular Imaging of Inflammatory Atheroma using Targeted Echogenic Immunoliposomes

**Hyunggun Kim**[a], **Patrick H. Kee**[a], **Yonghoon Rim**[a], **Melanie R. Moody**[a], **Melvin E. Klegerman**[a], **Deborah Vela**[b], **Shao-Ling Huang**[a], **David D. McPherson**[a], and **Susan T. Laing**[a]

[a]Division of Cardiology, Department of Internal Medicine, The University of Texas Health Science Center at Houston, Houston, TX

[b]Department of Pathology, The Texas Heart Institute, Houston, TX

## Abstract

**Objective:** This study aimed to demonstrate whether pretreatment with nitric oxide (NO) loaded into echogenic immunoliposomes (ELIP) plus ultrasound, applied before injection of molecularly targeted ELIP can promote penetration of the targeted contrast agent and improve visualization of atheroma components.

**Methods:** ELIP were prepared using the pressurization-freeze method. Atherosclerosis was induced in Yucatan miniswine by balloon denudation and a hyperlipidemic diet. The animals were randomized to receive anti-intercellular adhesion molecule-1 (ICAM-1) ELIP or immunoglobulin (IgG)-ELIP, and were subdivided to receive pretreatment with standard ELIP plus ultrasound, NO-loaded ELIP, or NO-loaded ELIP plus ultrasound. Intravascular ultrasound (IVUS) data were collected before and after treatment.

**Results:** Pretreatment with standard ELIP plus ultrasound or NO-loaded ELIP without ultrasound resulted in 9.2 ± 0.7% and 9.2 ± 0.8% increase in mean gray scale values, respectively, compared to baseline ($p<0.001$ vs. control). Pretreatment with NO-loaded ELIP plus ultrasound activation resulted in a *further* increase in highlighting with a change in mean gray scale value to 14.7 ± 1.0% compared to baseline ($p<0.001$ vs. control). These differences were best appreciated when acoustic backscatter data values (RF signal) were used [22.7 ± 2.0% and 22.4 ± 2.2% increase in RF signals for pretreatment with standard ELIP plus ultrasound and NO-loaded ELIP without ultrasound respectively ($p<0.001$ vs. control), and 40.0 ± 2.9% increase in RF signal for pretreatment with NO-loaded ELIP plus ultrasound ($p<0.001$ vs. control)].

**Conclusion:** NO-loaded ELIP plus ultrasound activation can facilitate anti-ICAM-1 conjugated ELIP delivery to inflammatory components in the arterial wall. This NO pretreatment strategy has potential to improve targeted molecular imaging of atheroma for eventual true tailored and personalized management of cardiovascular diseases.

### Keywords

Molecular Imaging; Atherosclerosis; Contrast Agent; Nitric Oxide; Ultrasound



Correspondence should be addressed to: Susan T. Laing, MD, MS Susan.T.Laing@uth.tmc.edu 6431 Fannin St., MSB 1.246, Houston, TX 77030 Phone: (713) 500-6630; Fax: (713) 500-6556.

## INTRODUCTION

Progression of atheroma to a vulnerable morphology, resulting in plaque rupture and activation of the extrinsic coagulation pathway, has been implicated in acute myocardial infarction and ischemic stroke [1-2]. Inflammation is thought to be a central mechanism for progression of atheroma from a stable lesion to a vulnerable plaque and its consequent clinical events. Much work has been done to develop molecularly targeted contrast agents for various imaging modalities [3-6], in order to identify atheroma and atheroma components with the eventual goal of identifying an atheroma's potential to progress to a vulnerable or otherwise dangerous pathological state. However, to date, there remains no clinically useful diagnostic methodology for staging atherosclerotic disease [7].

We have developed echogenic liposomes (ELIP) for targeted diagnostic and ultrasound-sensitive therapeutic controlled release applications [8-10]. The former application includes proof-of-principle staging of atheroma progression by B-mode intravascular ultrasound (IVUS) imaging of atheroma in the carotid and iliofemoral arteries using ELIP targeted to adhesion molecules in an early and mid-stage miniswine atherosclerosis model [11-12]. We have also found that both continuous wave and pulsed wave Doppler ultrasound enhances the penetration of drugs and stem cells into all layers of the arterial wall, whether released from or associated with ELIP [13-15].

Nitric oxide (NO) is a well-known vasodilator that also increases vascular wall permeability in animal models [16-17]. We have encapsulated NO into ELIP, producing a bioactive gas delivery vehicle characterized by a bimodal diffusive release profile and the ability to release its gas load instantaneously by application of either continuous wave or pulsed wave Doppler ultrasound [18-20]. This formulation was shown to inhibit atheroma progression in a rabbit model of neointimal hyperplasia [19] and to enhance the passage of ELIP-bound stem cells through an endothelial cell layer in vitro [21].

We hypothesize that administration of NO-loaded ELIP with applied ultrasound before injection of molecularly targeted ELIP will promote penetration of targeted ELIP into the arterial wall and improve visualization of atheroma components by combining the vascular wall permeability-enhancing mechanisms of ultrasound and NO. For these experiments, we utilized IVUS as an imaging modality and intercellular adhesion molecule-1 (ICAM-1) targeted ELIP to identify early and mid-stage inflammatory components of atheromas.

## MATERIALS AND METHODS

### ELIP Preparation

**Preparation of standard ELIP—**A 27:42:8:8:15 molar ratio of the lipid components L-α-phosphatidylcholine (chicken egg; EPC), 1,2-dipalmitoyl-sn-glycero-3-phosphocholine (DPPC), 1,2-dipalmitoyl-sn-glycero-3-[phosphor-rac-1-glycerol] (DPPG), 1,2-dipalmitoyl-sn-glycero-3-phosphoethanolamine (DPPE), and cholesterol (CH) were mixed in a round-bottom flask as chloroform solutions. The chloroform was then removed by evaporation under argon, while the flask was rotated in a 50°C water bath. The resulti ng lipid film was placed under vacuum for 4 hours at ≤100 mTorr pressure for complete removal of the solvent, followed by rehydration of the dry lipid film with 0.32 M mannitol to a concentration of 10 mg lipid/ml. The hydrated lipid was incubated at 55°C for 30 minutes to ensure that all lipids were in the liquid phase during hydration. The mixture was then sonicated in a water bath for 5 minutes. Aliquots of the suspension were frozen at −80°C and lyophilized for 24–48 hours. Each lyophilized dry cake was resuspended with the original volume of nanopure water immediately before use.

**Preparation of NO-loaded ELIP—**Liposomes of the above composition were prepared according to a previously developed pressurization-freeze method [22]. Briefly, after drying and hydrating the lipid film, 300-μl aliquots of the suspension were transferred to 2-ml borosilicate glass vials (12×32 mm), which were then sealed with Teflon-coated silicon rubber septal screw caps. Nitric oxide (5.4 ml STP), washed and purified by passage through a saturated sodium hydroxide solution in order to remove nitrogen dioxide produced by contaminating oxygen, or a mixture of NO and argon was introduced into each vial through the septum and pressurized to 9 atm using a syringe fitted with a 27G×1/2″ needle. The pressurized gas/liposome dispersion was incubated for 30 minutes at room temperature, followed by freezing on dry ice for ≥ 30 minutes. Vials were stored at −80° C. Prior to use, the pres sure was released by loosening the caps immediately after removal from storage, followed by thawing of the NO-loaded ELIP suspension at room temperature.

**Preparation of antibody-conjugated ELIP—**For conjugation, standard ELIP were prepared as described above, substituting 1,2-dipalmitoyl-sn-glycero-3-phosphoethanolamine-N-[4-(pmaleimidophenyl) butyrate] (MPB-PE) for PE. For protein thiolation, 0.4 mg monoclonal anti-human/porcine ICAM-1 (Neomarkers clone 15.2) and 1.6 mg nonspecific mouse Immunoglobulin G (IgG; Rockland Immunochem., Inc., Gilbertsville, PA) or 2 mg IgG alone were reacted with 3-(2-pyridyldithiolpropionic acid)-N-hydroxysuccinimide ester (SPDP) at a SPDP:IgG protein molar ratio of 15:1 for 30 min at 24 ± 1 °C. Protein was separated from unreacted SPDP by gel chromatography on a 50 ml Sephadex G-50 column (Sigma-Aldrich, St. Louis, MO, USA) equilibrated with 0.05M citrate-phosphate buffer at a pH of 5.5. Protein fractions were identified using a spectrophotometric technique (Genesys 10uv, Thermo Electron Corp., Milford, MA) at a wavelength of 280 nm, pooled and concentrated to ≤ 2 ml using Centricon YM-10 centrifugal filter units (Millipore, Billerica, MA, USA). The SPDP-activated protein was reduced in 25mM dithiothreitol (DTT) for 30 min at 24 ± 1 °C. The thiolated protein was isolated using a Sephadex G-50 column, equilibrated and eluted with pH 6.7 citrate-phosphate buffer. The thiolated protein was reacted with reconstituted MPB-ELIP (10mg lipid/ml 0.1 M phosphate buffer at a pH of 6.62) under argon overnight at 24 ± 1°C. Rh-ELIP were separated from free protein and low molecular weight products by gel filtration on a 20-ml Sepharose CL-4B column (Sigma-Aldrich) that had been pre-saturated with unconjugated, unlabeled ELIP according to the method of Lasch et al [23], and eluted with 0.02 M phosphate-buffered saline (PBS) at a pH of 7.4. Liposome-containing fractions were identified by optical absorbance at a wavelength of 440 nm prior to elution of free IgG. The IgG- or anti-ICAM-1-ELIP were lyophilized with 0.1M D-mannitol.

## Animal Model

All animal experiments were approved by the Animal Welfare Committee at the University of Texas Health Science Center at Houston. Atherosclerosis was induced in Yucatan Miniswine with a standard procedure of combined balloon denudation and a hyperlipidemic diet [24]. Briefly, Yucatan miniswine were given a hyperlipidemic diet containing 2% cholesterol and 15% lard. After two weeks, the animals underwent the denudation procedures. Under sterile conditions, the animals were anesthetized with ketamine (35 mg/kg), xylazine (5 mg/kg) and 1% to 3% inhaled isoflurane. Under fluoroscopic guidance, a 4F Fogarty catheter was inserted into the right carotid artery and advanced to the iliofemoral arteries. The balloon tip of the 4F Fogarty catheter was inflated with diluted iodixanol (Visipaque) solution to aid in its visualization under fluoroscopy and the catheter pulled back and forth twice to denude the arterial endothelium. Similarly, the carotid artery was also denuded before the catheter was removed and incision was sutured. The animal continued to receive a hyperlipidemic diet for another 45 days before undergoing the imaging experiments described below.

### Imaging Procedure

The animals were similarly anesthetized as described above. A 6 Fr sheath was inserted into both femoral arteries. For intravascular ultrasound (IVUS) imaging, a 3.5F Eagle Eye Gold IVUS catheter (20 MHz, Volcano Corporation, San Diego, CA) was utilized with a Volcano s5i Imaging System (Volcano Corporation, San Diego, CA). The IVUS catheter was inserted through the arterial sheath via the left or right femoral arterial sheath and advanced retrogradely past the region of injury to image the iliofermoral or carotid arterial segments of interest. IVUS data of the arterial segment of interest were obtained using an automatic pullback device at a constant speed of 0.5 mm/s and continuously recorded in digital format. Images were obtained at baseline and after 5 minutes after ELIP treatment as described below. Instrument settings for gain and zoom levels in the IVUS system were set such that the luminal border and the arterial wall structure were visibly detectable at baseline for each artery. These settings remained constant throughout IVUS imaging. At the end of the procedure, the animals were sacrificed and the arteries were harvested for histological analysis.

### ELIP Treatment

The animals were randomized into 2 experimental groups: treatment with anti-ICAM-1 ELIP or control IgG-ELIP. Each experimental group was then subdivided to receive pretreatment with either standard ELIP (air containing ELIP without NO) plus ultrasound, NO-loaded ELIP without ultrasound, or NO-loaded ELIP plus ultrasound (n=3 arteries per group; Figure 1). Contrast agent delivery was performed via a catheter with a central lumen introduced retrogradely via the femoral arterial sheaths. IVUS data of the same arterial segments were collected before and after treatment. For arteries receiving ultrasound pretreatment, ultrasound was delivered using a 12-MHz vascular transducer (HDI 5000, Philips Healthcare, Andover, MA) placed over the iliofemoral or carotid artery in parallel with blood flow direction. Color Doppler ultrasound (Doppler frequency = 6 MHz, pulse repetition frequency = 5 kHz, mechanical index = 0.4) was utilized to facilitate NO release from NO-ELIP.

### Quantification of IVUS data and 3D IVUS visualization

Amplitude envelope was retrieved from the IVUS signal data using the Hilbert transform, and utilized to reconstruct data sets (i.e., acoustic backscatter) in the polar coordinate consisting of the radial and circumferential axes [25]. IVUS signal envelope data were collected at 1,024 data points per scan line and 256 scan lines along 360 degree per IVUS slice (Eagle Eye Gold catheter, Volcano Corporation, San Diego, CA). The acoustic backscatter data sets in the polar coordinate were transformed to the Cartesian coordinate system for standard IVUS imaging [25]. Since the arterial segments evaluated were relatively straight, it was assumed that the pullback direction of IVUS catheter was in parallel with the longitudinal direction of the artery.

We utilized our graphical user interface (GUI)-based image processing system developed particularly for interactive tracing and segmenting procedures under MATLAB (Mathworks Inc., Natick, MA) platform. The endothelium/atheroma border and the outer edge of the dense adventitia in each IVUS slice were manually segmented, and the acoustic enhancement within the arterial wall borders following each treatment was quantitated by both mean gray scale values (i.e. pixelated data) and acoustic backscatter values (i.e. signal data).

A series of segmented images of the artery (total of 15 IVUS slices over the length of the artery imaged) was placed in a tomographic sequence along the longitudinal direction (10 cm in length) for 3-dimensional (3D) reconstruction. The gray scale values and radio

frequency (RF) data within the arterial wall borders were utilized to calculate averaged acoustic enhancement data along the radial direction (for a total of 256 scan lines in the polar coordinate) of the arteries. First, 3D mapped images of the arteries reconstructed were created using both gray scale and RF data to better visualize and compare the extent and distribution of the highlighted regions of interest across the arterial structure between treatment groups. These data were presented with respect to the longitudinal direction (i.e. blood flow direction) and the circumferential direction of the artery. Secondly, we performed volumetric 3D IVUS reconstruction of the arteries using our shape-based nonlinear interpolation method [25]. Image stacks containing 144 IVUS slice images were utilized to generate volumetric 3D IVUS images.

### Histology

Following euthanasia, arteries were harvested and segments were either frozen or fixed in 4% formalin. Arteries were cut into 5mm segments, embedded in paraffin, and cut into 5 μm slices. Staining by immunohistochemistry was performed using a custom polyclonal anti-ICAM-1 antibody expressed against porcine tissue (abMART Co., LTD; 1:1000 dilution). Adjacent sections were stained with a modified Movat's pentochrome. With this staining protocol, elastic tissue stains black, fibrous tissue stains blue-green, and cell cytoplasm stains red.

### Quantitative real-time RT-PCR

Gene expression levels of ICAM-1 were determined using quantitative real-time reverse transcriptase polymerase chain reaction (RT-PCR). Total RNA was isolated from frozen tissue using a commercially available kit (RiboPure kit, Applied Biosystems, Foster City, USA). RNA yield and purity were measured and 1 μg RNA was subsequently used for the synthesis of cDNA using the MultiScribe™ Reverse Transcriptase System (Applied Biosystems, Foster City, USA). Quantitative PCR was then performed using 2 μl of undiluted cDNA, the TaqMan Universal PCR Master Mix (Applied Biosystems, Foster City, USA) and a Taqman Gene expression assay for pig ICAM-1 (Applied Biosystems, Foster City, USA). Negative controls containing 2 μl of nuclease free $H_2O$ in place of cDNA were included. Data were normalized to an endogenous reference gene (eukaryotic 18S, Applied Biosystems, Foster City, USA) and presented as number-fold change in gene expression relative to the uninjured, untreated internal control ($2^{-\Delta\Delta C}{}_T$ method).

### Statistical analysis

SigmaStat (Systat Software Inc, Point Richmond, CA) was utilized for data analysis. Data are reported as percent change in highlighting compared to baseline (n=3 arteries per group; 15 IVUS slices per artery). For comparison of treatment groups, t-test or analysis of variance was used for parametric data and the Kruskal-Wallis analysis of variance of ranks or median test for nonparametric data. Pairwise differences between groups were analyzed using the Dunn's Method. Data were plotted as mean and standard error. A P-value of 0.05 was considered as statistically significant.

## RESULTS

Figure 2 demonstrates a representative artery with inflammatory atheroma. There was expression of the inflammatory marker ICAM-1 in the neointima and the arterial wall (Figure 3). Using quantitative PCR, there was a 20-30-fold increase in ICAM expression for the carotid and iliofemoral arteries compared to control (uninjured and untreated) arteries. There was no difference in ICAM expression between arteries pretreated with NO-ELIP and those that were not (21.8 fold increase vs. 26.6 fold increase, $p>0.05$).

Immunohistochemistry of the arteries pretreated with or without NO-ELIP also showed no differences in ICAM staining.

There was significant highlighting when arteries were treated with anti-ICAM-1-conjugated ELIP when compared to IgG-conjugated ELIP regardless of pretreatment strategy used [11.0 ± 1.8% vs. 5.1 ± 0.5% ($p=0.03$) for MGSV and 28.0 ± 5.5% vs. 7.9 ± 0.6% ($p=0.02$) for RF data]. There was no significant highlighting demonstrated by IgG-conjugated ELIP compared to baseline ($p>0.05$). There was also no statistical difference among arteries treated with IgG-conjugated ELIP when pretreated with standard ELIP plus ultrasound, NO-loaded ELIP without ultrasound, or NO-loaded ELIP plus ultrasound ($p>0.05$; Figure 4). Hence, for subsequent analyses, all data for IgG-conjugated ELIP-treated arteries were compiled as control.

Pretreatment with standard ELIP plus ultrasound and NO-loaded ELIP without ultrasound resulted in 9.2 ± 0.7% and 9.2 ± 0.8% increase in mean gray scale values, respectively, compared to baseline ($p<0.001$ vs. IgG-ELIP; Figure 4). Pretreatment with both NO-loaded ELIP plus ultrasound activation resulted in a *further* increase in highlighting with a change in mean gray scale value to 14.7 ± 1.0% compared to baseline ($p<0.001$ vs. IgG-ELIP and $p<0.05$ compared to pretreatment with standard ELIP or NO-loaded ELIP; Figures 4 & 5). These differences were best appreciated when acoustic backscatter data values (RF signal) were used rather than gray scale values (Figures 4 & 5). There was a 22.7 ± 2.0% and 22.4 ± 2.2% increase in RF signals for pretreatment with standard ELIP plus ultrasound and NO-loaded ELIP without ultrasound respectively ($p<0.001$ vs. IgG-ELIP; Figure 4). Pretreatment with NO-loaded ELIP plus ultrasound activation however, resulted in a 40.0 ± 2.9% increase in RF signal intensity compared with baseline ($p<0.001$ vs. IgG-ELIP and $p<0.05$ compared to pretreatment with standard ELIP or NO-loaded ELIP; Figure 4).

Figure 6 demonstrates representative 3D mapped images of the arteries treated with IgG-conjugated ELIP vs. those pretreated with NO-loaded ELIP plus ultrasound activation followed by anti-ICAM-1 conjugated ELIP. The x- and y-axes refer to the longitudinal and radial directions of the artery, respectively. Gray scale images showed no significant enhancement of highlighting between baseline and treatment for the IgG-conjugated ELIP group. For the anti-ICAM-1 conjugated ELIP treatment group with pretreatment of NO-loaded ELIP plus ultrasound activation however, there was enhanced highlighting demonstrated across the entire arterial structure compared to baseline (Figure 6). Landmarks of arterial bifurcation in the 3D mapped images of both baseline and treatment indicate that the 3D registration has been properly performed. The RF data images further demonstrate this enhanced highlighting seen with a pretreatment strategy of NO-loaded ELIP plus ultrasound activation (Figure 6).

Volumetric 3D IVUS images of representative arteries are shown in Figure 7. Our shape-based nonlinear interpolation method demonstrated realistic volumetric geometry of the arterial segment and acoustic backscatter distribution across the artery. While IgG-ELIP treatment showed little difference compared to baseline, pretreatment with NO-loaded ELIP plus ultrasound activation followed by anti-ICAM-1-ELIP treatment demonstrated markedly enhanced highlighting of inflammatory atherosclerotic components across the entire arterial segment for both outer and luminal surfaces of the artery compared to baseline.

## DISCUSSION

Pretreatment of NO-loaded ELIP plus ultrasound activation followed by anti-ICAM-1 ELIP treatment demonstrated significant acoustic enhancement indicating that delivery of NO to atherosclerotic arterial tissue facilitated vascular wall permeability and promoted penetration

of the subsequent targeted ELIP into the arterial wall. Although the gray scale image data demonstrated the effect of NO-loaded ELIP pretreatment on highlighting of atheroma components, RF data provided further detailed information pertaining to intensity distribution in the arterial wall. RF data analysis can help us more specifically and spatially differentiate highlighted regions of interest allowing improved molecular ultrasound imaging of atherosclerosis by targeted ELIP.

Many molecularly targeted imaging contrast agents are in various stages of clinical development with the expectation that they will improve the ability to detect and characterize pathologic structures, the overall aim of which is to enhance disease diagnosis and treatment. We have previously demonstrated enhanced IVUS and transvascular ultrasound imaging of atheroma and thrombi in vivo with ELIP conjugated to antibodies specific for various atheroma components [11-12, 24, 26]. We have also previously demonstrated that 1 MHz continuous wave ultrasound promotes penetration of liposomally encapsulated calcein, a drug surrogate, into all layers of the arterial wall [15], as well as penetration of intact rhodamine-labeled, ICAM-1-targeted ELIP into the aortic tunica media; we hypothesize that ultrasound activation increases transport of liposomes and drugs through endothelial tight junctions by nucleating stable cavitation [14]. In this study, we describe a novel pretreatment strategy using NO-loaded ELIP plus ultrasound activation for improved highlighting of atheroma.

Besides its striking vasodilatory effects, NO is also known to mediate increased vascular permeability secondary to inflammatory processes; however it is not known whether NO directly affects endothelial junctions or simply increases flow through the vasa vasorum [27-28]. Our hypothesis that NO-loaded ELIP could be combined with the vascular permeability-enhancing effects of ultrasound to improve the imaging enhancement afforded by targeted ELIP, has been supported by the results reported here. Pretreatment of NO-loaded ELIP plus ultrasound, followed by anti-ICAM-1 ELIP treatment, demonstrated significant acoustic enhancement, indicating that delivery of NO to atherosclerotic arterial tissue facilitated vascular wall permeability and promoted penetration of the targeted ELIP into the arterial wall.

Application of ultrasound during NO-ELIP pretreatment prior to administration of the targeted ELIP served to combine enhanced vascular permeability with liposomal fragmentation and immediate release of the entire gas payload. In addition, we confirmed that color Doppler ultrasound, utilizing parameters previously shown to be effective in promoting tissue plasminogen activator (tPA)-loaded ELIP thrombolysis in vivo [22, 29], is as effective as continuous wave ultrasound in promoting penetration of ELIP into the arterial wall, this time for diagnostic imaging. Although the gray scale image data demonstrated the effect of NO-ELIP pretreatment on highlighting of atheroma components, RF signal data provided further detailed information pertaining to intensity distribution within the arterial wall.

One limitation of the study is that intraarterial injection of the ELIP was performed which may limit the clinical applications of this pretreatment strategy. Although we have shown transpulmonary transit of our ELIP as well as effective ELIP delivery via intravenous injection in a small animal model [30], delivery to the peripheral arteries in a large animal model is variable [31]. Since this is our first report of this novel pretreatment strategy for molecular imaging, we chose to use the intraarterial delivery route for this study. Clinical translation of an intraarterial delivery strategy however, is provided by routine coronary and peripheral arterial angiographies. Another limitation is that we chose to use a 60-day atherosclerotic miniswine model and did not evaluate more advanced atherosclerotic lesions (i.e., a 120-day atherosclerotic model). Hence the effect of this NO-ELIP pretreatment

strategy cannot be extrapolated to more advanced and potentially calcified lesions. This study was designed to evaluate improvement in highlighting of one molecular targeting agent (anti-ICAM-1 ELIP) and we did not evaluate highlighting using other atheroma components.

In summary, NO-loaded ELIP when combined with ultrasound activation can effectively improve endothelial permeability facilitating anti-ICAM-1 conjugated ELIP delivery to inflammatory components in the arterial wall. This NO pretreatment strategy has a potential to improve targeted molecular imaging for early and mid-stage atheroma. Clinical applications could include serial evaluation of atheroma progression, assessment of the molecular effects of biotherapeutics particularly in the preclinical stage, and the early detection of rupture-prone plaques leading to improved preventive strategies. These efforts may eventually pave the way for true personalized medicine as atherosclerosis diagnosis and therapy are tailored to a patient's unique molecular signature.

## Acknowledgments

Supported by the National Institutes of Health RO1 HL-059786 and HL-74002

## References

1. Eldrup N, Gronholdt ML, Sillesen H, Nordestgaard BG. Elevated matrix metalloproteinase-9 associated with stroke or cardiovascular death in patients with carotid stenosis. Circulation. 2006; 114:1847–1854. [PubMed: 17030690]
2. Naghavi M, Libby P, Falk E, Casscells SW, Litovsky S, Rumberger J, et al. From vulnerable plaque to vulnerable patient: a call for new definitions and risk assessment strategies: Part I. Circulation. 2003; 108:1664–1672. [PubMed: 14530185]
3. Kornmann LM, Reesink KD, Reneman RS, Hoeks AP. Critical appraisal of targeted ultrasound contrast agents for molecular imaging in large arteries. Ultrasound Med Biol. 2010; 36:181–191. [PubMed: 20018434]
4. Lindner JR. Molecular imaging of cardiovascular disease with contrast-enhanced ultrasonography. Nat Rev Cardiol. 2009; 6:475–481. [PubMed: 19506587]
5. Sadat U, Li ZY, Graves MJ, et al. Noninvasive imaging of atheromatous carotid plaques. Nat Clin Pract Cardiovasc Med. 2009; 6:200–209. [PubMed: 19234500]
6. Cormode DP, Roessl E, Thran A, et al. Atherosclerotic plaque composition: analysis with multicolor CT and targeted gold nanoparticles. Radiology. 2010; 256:774–782. [PubMed: 20668118]
7. Drakopoulou M, Toutouzas K, Michelongona A, Tousoulis D, Stefanadis C. Vulnerable plaque and inflammation: potential clinical strategies. Curr Pharm Des. 2011; 17:4190–4209. [PubMed: 22204378]
8. Alkan-Onyuksel H, Demos SM, Lanza GM, Vonesh MJ, Klegerman ME, Kane BJ, et al. Development of inherently echogenic liposomes as an ultrasonic contrast agent. J Pharm Sci. 1996; 85:486–490. [PubMed: 8742939]
9. Huang S, Hamilton AJ, Tiukinhoy SD, Nagaraj A, Kane BJ, Klegerman M, et al. Liposomes as ultrasound imaging contrast agents and as ultrasound-sensitive drug delivery agents. Cell Mol Biol Lett. 2002; 7:233–235. [PubMed: 12097929]
10. Huang SL. Liposomes in ultrasonic drug and gene delivery. Adv Drug Deliv Rev. 2008; 60:1167–1176. [PubMed: 18479776]
11. Demos SM, Alkan-Onyuksel H, Kane BJ, Ramani K, Nagaraj A, Greene R, et al. In vivo targeting of acoustically reflective liposomes for intravascular and transvascular ultrasonic enhancement. J Am Coll Cardiol. 1999; 33:867–875. [PubMed: 10080492]
12. Hamilton AJ, Huang SL, Warnick D, Rabbat M, Kane B, Nagaraj A, et al. Intravascular ultrasound molecular imaging of atheroma components in vivo. J Am Coll Cardiol. 2004; 43:453–460. [PubMed: 15013130]

13. Herbst SM, Klegerman ME, Kim H, Qi J, Shelat H, Wassler M, et al. Delivery of stem cells to porcine arterial wall with echogenic liposomes conjugated to antibodies against CD34 and intercellular adhesion molecule-1. Mol Pharm. 2010; 7:3–11. [PubMed: 19719324]
14. Hitchcock KE, Caudell DN, Sutton JT, Klegerman ME, Vela D, Pyne-Geithman GJ, et al. Ultrasound-enhanced delivery of targeted echogenic liposomes in a novel ex vivo mouse aorta model. J Control Release. 2010; 144:288–295. [PubMed: 20202474]
15. Laing ST, Kim H, Kopechek JA, Parikh D, Huang S, Klegerman ME, et al. Ultrasound-mediated delivery of echogenic immunoliposomes to porcine vascular smooth muscle cells in vivo. J Liposome Res. 2010; 20:160–167. [PubMed: 19842795]
16. Meijer F, Ruijter JM, Van Delft JL, Van Haeringen NJ. Nitric oxide induces vascular permeability changes in the guinea pig conjunctiva. Eur J Pharmacol. 1995; 284:61–67. [PubMed: 8549637]
17. Moncada S, Higgs A. The L-arginine-nitric oxide pathway. N Engl J Med. 1993; 329:2002–2012. [PubMed: 7504210]
18. Huang SL. Ultrasound-responsive liposomes. Methods Mol Biol. 2010; 605:113–128. [PubMed: 20072876]
19. Huang SL, Kee PH, Kim H, Moody MR, Chrzanowski SM, MacDonald RC, et al. Nitric oxide-loaded echogenic liposomes for nitric oxide delivery and inhibition of intimal hyperplasia. J Am Coll Cardiol. 2009; 54:652–659. [PubMed: 19660697]
20. Huang SL, McPherson DD, Macdonald RC. A method to co-encapsulate gas and drugs in liposomes for ultrasound-controlled drug delivery. Ultrasound Med Biol. 2008; 34:1272–1280. [PubMed: 18407399]
21. Klegerman ME, Wassler M, Huang SL, Zou Y, Kim H, Shelat S, et al. Liposomal modular complexes for simultaneous targeted delivery of bioactive gases and therapeutics. J Control Release. 2010; 142:326–331. [PubMed: 19903503]
22. Laing ST, Moody MR, Kim H, Smulevitz B, Huang SL, Holland CK, et al. Thrombolytic efficacy of tissue plasminogen activator-loaded echogenic liposomes in a rabbit thrombus model. Thromb Res. 2012; 130:629–635. [PubMed: 22133272]
23. Lasche, J.; Weissig, V.; Brandl, M. Preparation of liposomes. In: Torchilin, VP.; Weissig, V., editors. Liposomes. Vol. 2003. Oxford University Press; New York, NY: p. 24-25.
24. Kim H, Moody MR, Laing ST, Kee PH, Huang SL, Klegerman ME, et al. In vivo volumetric intravascular ultrasound visualization of early/inflammatory arterial atheroma using targeted echogenic immunoliposomes. Invest Radiol. 2010; 45:685–691. [PubMed: 20733507]
25. Rim Y, McPherson DD, Kim H. Volumetric three-dimensional intravascular ultrasound visualization using shape-based nonlinear interpolation. BioMedical Enginerring Online. 2013; 12:39.
26. Hamilton A, Huang SL, Warnick D, Stein A, Rabbat M, Madhav T, et al. Left ventricular thrombus enhancement after intravenous injection of echogenic immunoliposomes: studies in a new experimental model. Circulation. 2002; 105:2772–2778. [PubMed: 12057993]
27. Breithaupt-Faloppa AC, Vitoretti LB, Coelho FR, dos Santos Franco AL, Domingos HV, Sudo-Hayashi LS, et al. Nitric oxide mediates lung vascular permeability and lymph-borne IL-6 after an intestinal ischemic insult. Shock. 2009; 32:55–61. [PubMed: 18838940]
28. Duran WN, Breslin JW, Sanchez FA. The NO cascade, eNOS location, and microvascular permeability. Cardiovasc Res. 2010; 87:254–261. [PubMed: 20462865]
29. Laing ST, Moody M, Smulevitz B, Kim H, Kee P, Huang S, et al. Ultrasound-enhanced thrombolytic effect of tissue plasminogen activator-loaded echogenic liposomes in an in vivo rabbit aorta thrombus model--brief report. Arterioscler Thromb Vasc Biol. 2011; 31:1357–1359. [PubMed: 21441137]
30. Britton GL, Kim H, Kee PH, Aronowski J, Holland CK, McPherson DD, et al. In Vivo Therapeutic Gas Delivery for Neuroprotection with Echogenic Liposomes. Circulation. 2010; 122(16):1578–1587. [PubMed: 20921443]
31. Hamilton A, Huang SL, Warnick D, Stein A, Rabbat M, Madhav T, et al. Left ventricular thrombus enhancement after intravenous injection of echogenic immunoliposomes: studies in a new experimental model. Circulation. 2002; 105(23):2772–2778. [PubMed: 12057993]

## HIGHLIGHTS

- Molecular imaging of atheroma is improved by nitric oxide pretreatment with ultrasound activation
- Acoustic backscatter data provided detailed intensity distribution of molecular imaging agents
- This nitric oxide pretreatment strategy has potential to improve targeted molecular imaging

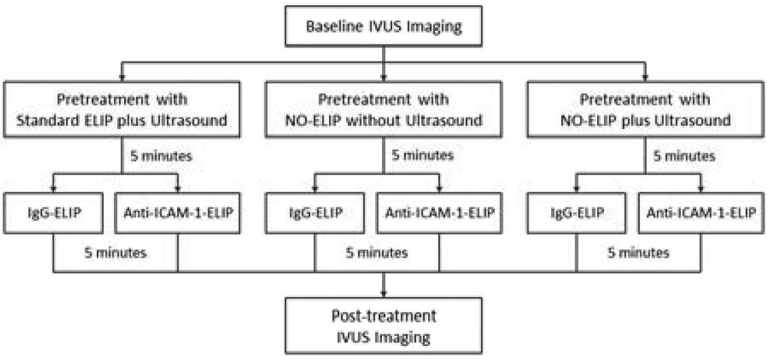


**Figure 1.**
Design flowchart demonstrating ELIP treatment groups.

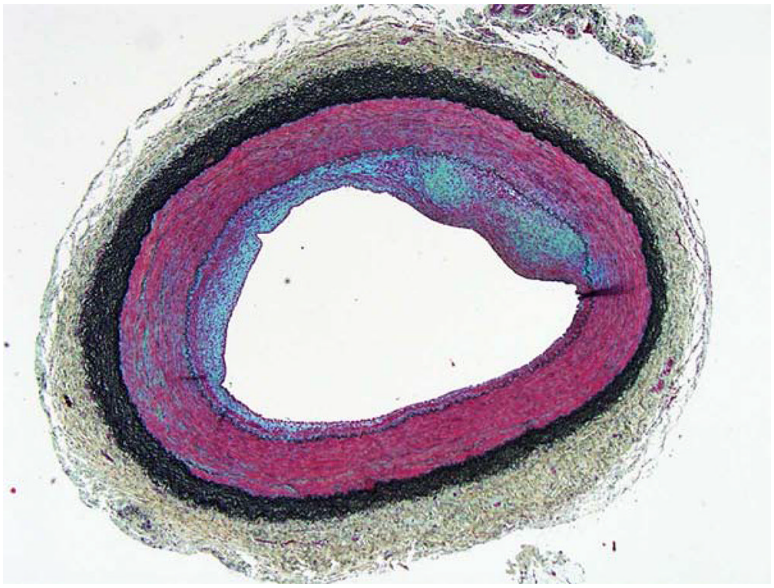

**Figure 2.**
Representative inflammatory atheroma in the Yucatan miniswine (Movat's staining: red=smooth muscle cell or endothelial cell, black=elastic fibers, blue-green=extracellular matrix).

**Figure 3.**
Representative inflammatory atheroma showing ICAM-1 expression. Movat's staining on the left (red=smooth muscle cell or endothelial cell, black=elastic fibers, blue-green=extracellular matrix) and custom ICAM-1 staining on the right (brown=ICAM).

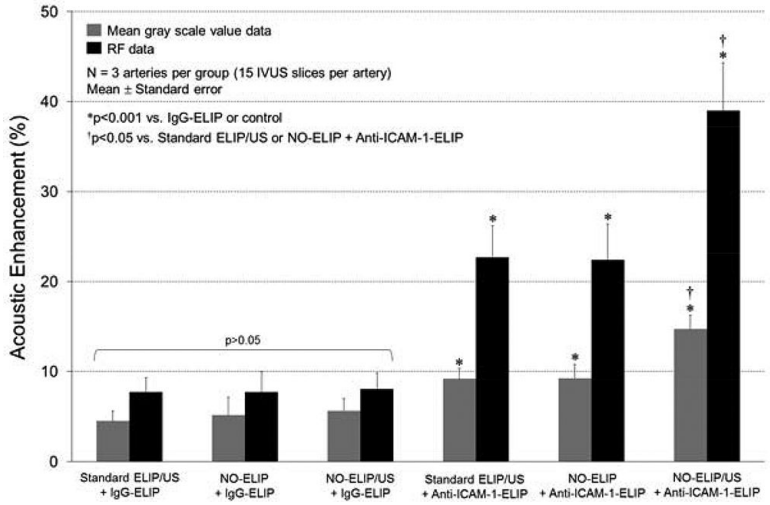


**Figure 4.**

Percent acoustic enhancement expressed as the increase in MGSV and RF signal compared to baseline for the different treatment groups. Data are presented as mean ± standard error.

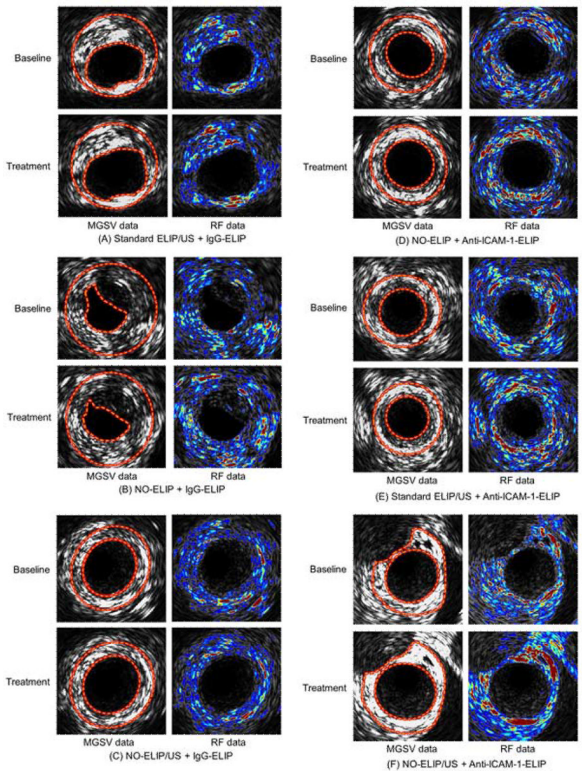


**Figure 5.**
Arterial segments showing gray scale images and RF data for all treatment groups.

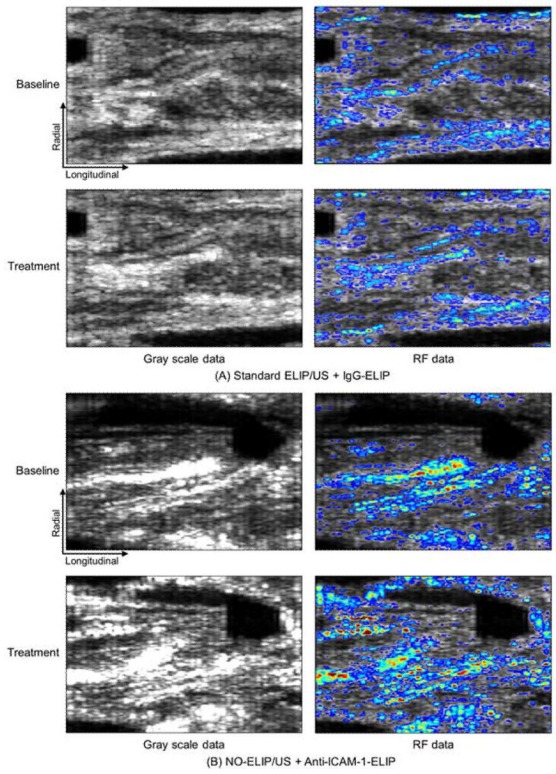


**Figure 6.**
Representative 3D mapped images of the arteries (IgG- ELIP vs. NO-ELIP/US + anti-ICAM-1-ELIP) using gray scale and RF data.

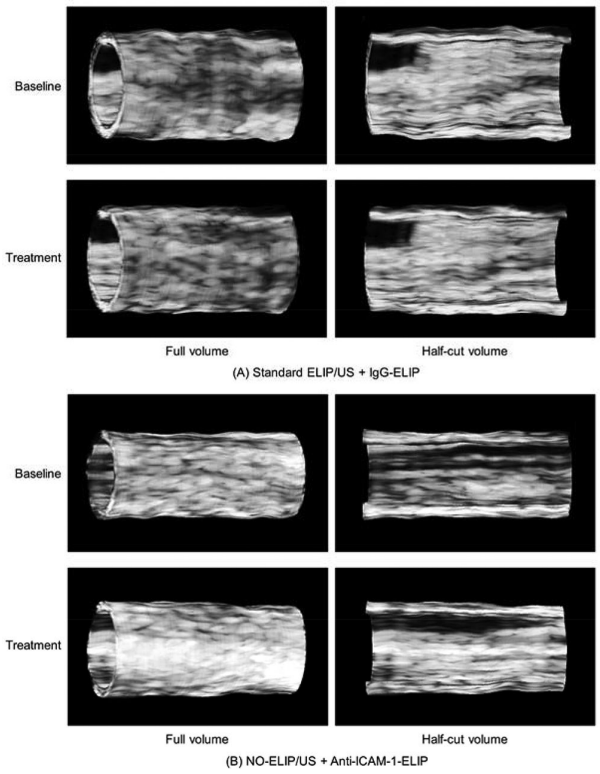


**Figure 7.**
Volumetric 3D reconstruction of a representative artery showing the degree of highlighting along the entire arterial segment of interest.